How Is the Active Site of Enolase Organized To Catalyze Two Different Reaction Steps?

Haiyan Liu,[†,‡] Yingkai Zhang,[†] and Weitao Yang*[,†]

Contribution from the Department of Chemistry, Duke University, Durham, North Carolina 27708, and School of Life Science, University of Science and Technology of China, Hefei, Anhui, 230026, China

Received October 12, 1999. Revised Manuscript Received April 19, 2000

Abstract: Using a combined ab initio quantum mechanical/molecular mechanical approach developed in our laboratory, we obtained the reaction paths and free energy barriers for the two steps of the reaction catalyzed by enolase. In the first step, the α-proton of the substrate, 2-phospho-D-glycerate (PGA), is removed by Lys345, resulting in an enolic intermediate. In the second step, the β-hydroxyl group leaves the enolic intermediate with the assistance of a general acid, Glu211. The calculated free energies of activation are 13.1 and 9.4 kcal mol^{-1} for the first and the second step, respectively. The barrier heights are consistent with the reaction rates measured from experiments. The calculations indicate that the electrostatic interactions between the substrate and two divalent metal cations at the active site strongly favor the first step. However, the same metal cations strongly disfavor the second step because the change in charge of the substrate is of an opposite sign compared with that in the first step. We conclude that the enzyme environment (excluding Lys345, Glu211, and the metal cations) forms an essential part of the reaction mechanism. It counterbalances the disfavoring effects of the metal cations in the second step without interfering with the first step despite the reversed charge changes of the substrate in the two steps. This capability of the enzyme originates from the three-dimensional organization of polar and charged groups in the active site of enolase, as indicated by correlations between the three-dimensional structure and energetic analyses based on our calculations. To achieve overall catalytic efficiency, the structure of the enolase active site takes advantage of the fact that the charge reorganization procedures accompanying the two reaction steps take place in two different directions in space.

I. Introduction

It is a common belief that enzymes carry out catalysis by preferentially stabilizing the transition states.[1−3] However, when it comes to a specific enzyme, it is not always obvious what particular features of the enzyme provide the stabilization and how. One theory is that the transition-state stabilizing effects are mainly of electrostatic nature.[2,4] Other factors are also frequently discussed in the literature.[5] In this paper, we will consider enolase, an enzyme that has been extensively studied by experiments and calculations. It belongs to an enzyme superfamily that, with a variety of other enzymes, shares a common feature of catalyzing reactions initialized with the abstraction of an α-proton from a carboxylic acid substrate.[6,7] Enolases in particular catalyze the dehydration of **1**, 2-phospho-D-glycerate (PGA), to form **3**, phosphoenolpyruvate (PEP)[8,9] (Scheme 1). Enolases are mostly homodimers and require two divalent metal ions per monomer for activity.[10,11]

A stepwise mechanism has emerged from previous studies of the enolase-catalyzed dehydration reaction (Scheme 1).[11−25] The first step involves the abstraction of the proton on carbon-2 of PGA (the α-proton) by a general base of the enzyme. The second step is the leaving of the hydroxyl group on carbon-3

[†] Duke University.
[‡] University of Science and Technology of China.

(1) Kraut, J. *Science* **1988**, *242*, 533−540.
(2) Warshel, A.; Aqvist, J.; Creighton, S. *Proc. Natl. Acad. Sci. U.S.A.* **1989**, *86*, 5820−5824.
(3) Knowles, J. R. *Nature* **1991**, *350*, 121−124.
(4) Warshel, A.; Florian, J. *Proc. Natl. Acad. Sci. U.S.A.* **1998**, *95*, 5950−5955.
(5) Fersht, A. *Enzyme structure and mechanism;* Freeman: New York, 1985.
(6) Gerlt, J. A.; Gassman, P. G. *J. Am. Chem. Soc.* **1992**, *114*, 5928−5934.
(7) Babbitt, P. C.; Hasson, M. S.; Wedekind, J. E.; Palmer, D. R. J.; Barrett, W. C.; Reed, G. H.; Ringe, I. R. D.; Kenyon, G. L.; Gerlt, J. A. *Biochemistry* **1996**, *35*, 16489−16501.
(8) Wold, F.; Ballou, C. E. *J. Biol. Chem.* **1957**, *227*, 301−312.
(9) Wold, F.; Ballou, C. E. *J. Biol. Chem.* **1957**, *227*, 313−328.
(10) Faller, L. D.; Baroudy, B. M.; Johnson, A. M.; Ewall, R. X. *Biochemistry* **1977**, *16*, 3684−3689.
(11) Poyner, R. R.; Reed, G. H. *Biochemistry* **1992**, *31*, 7166−7173.
(12) Reed, G. H.; Poyner, P. R.; Larsen, T. M.; Wedekind, J. E.; Rayment, I. *Curr. Opin. Struct. Biol.* **1996**, *6*, 736−743.
(13) Larsen, T. M.; Wedekind, J. E.; Rayment, I.; Reed, G. H. *Biochemistry* **1996**, *35*, 4349−4358.
(14) Duquerroy, S.; Camus, C.; Janin, J. *Biochemistry* **1995**, *34*, 12513−12523.
(15) Wedekind, J. E.; Reed, G. H.; Rayment, I. *Biochemistry* **1995**, *34*, 4325−4330.
(16) Wedekind, J. E.; Reed, G. H.; Rayment, I. *Biochemistry* **1994**, *33*, 9333−9342.
(17) Zhang, E.; Hatadam, J. M.; Brewer, J. M.; Lebioda, L. *Biochemistry* **1994**, *33*, 6295−6300.
(18) Lebioda, L.; Stec, B. *Biochemistry* **1991**, *30*, 2817−2822.
(19) Anderson, S. R.; Anderson, V. E.; Knowles, J. R. *Biochemistry* **1994**, *33*, 10545−10555.
(20) Vinarov, D. A.; Nowak, T. *Biochemistry* **1998**, *37*, 15238−15246.
(21) Brewer, J. M.; Clover, C. V. C.; Holland, M. J.; Lebioda, L. *Biochem. Biophys. Act.* **1998**, 1383, 351−355.
(22) Brewer, J. M.; Glover, C. V. C.; Holland, M. J.; Lebioda, L. *Biochem. Biophys. Act.* **1997**, 1340, 88−96.
(23) Poyner, R. R.; Laughlin, L. T.; Reed, G. H. G. A. S. *Biochemistry* **1996**, *35*, 1692−1699.
(24) Sangadala, V. S.; Glover, C. V. C.; Robson, R.; Holland, M. J.; Lebioda, L.; Brewer, J. M. *Biochem. Biophys. Act.* **1995**, *1251*, 23−31.
(25) Brewer, J. M.; Robson, R. L.; Glover, C. V. C.; Holland, M. J.; Lebioda, L. *Proteins: Struct. Funct. Genet.* **1993**, *17*, 426−434.

10.1021/ja9936619 CCC: $19.00
Published on Web 06/30/2000

Scheme 1

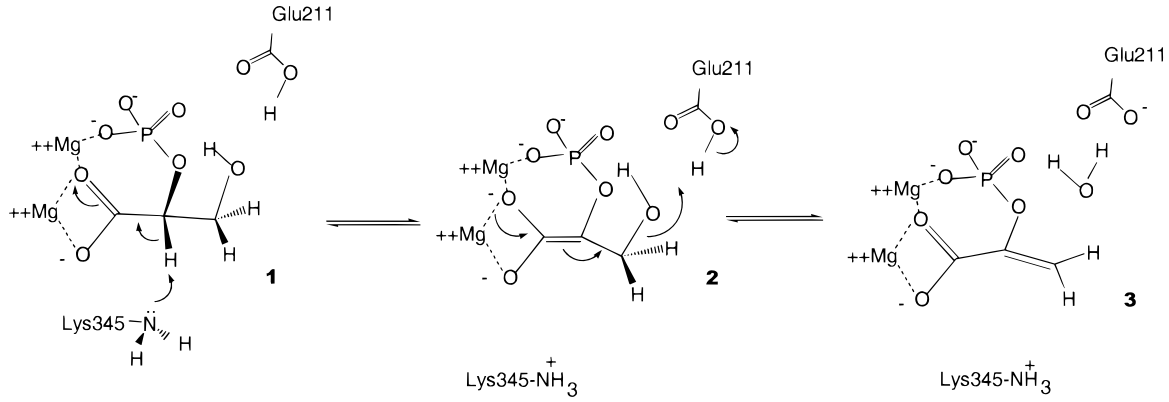

(the β-hydroxyl group) from **2**, an enolic intermediate, with the assistance of a general acid.

The first question of general interest about the stepwise mechanism is how the weakly acidic α-proton can be removed by a weakly basic enzyme group. This question is common to the mechanisms of other members of the enolase superfamily. Enolase is the only member of the enolase superfamily known to require two divalent metal ions for catalysis. Crystal structure studies have revealed that two divalent metal cations are directly coordinated with the carboxyl and phosphate groups of the substrate.[13,26] It is commonly believed that the strong electrostatic/electrophilic interactions with these metal cations (and possibly some positively charged residues around the substrate) may sufficiently lower the pK_a of the α-proton.[6,27] A recent theoretical study based on a combined semiempirical quantum mechanical/molecular mechanical potential energy function focusing on the abstraction of the α-proton supported this proposition.[28]

The second question, which has not been addressed as much as the first one, relates to the leaving of the β-hydroxyl group. Provided that the strong interactions between the substrate and the metal ions persist throughout the reaction, the second step should be strongly disfavored by the metal cations because it involves removing a unit negative charge from the substrate. The question is whether this is the case, and if it is, how the second step can still proceed. To answer this question, it may be insufficient to consider only the metal cations and the catalytic acid/base groups.

In this work, we use a newly developed computational procedure to study the reaction catalyzed by enolase.[29,30] Computer simulations of enzyme reactions using combined quantum mechanical/molecular mechanical (QM/MM) models have attracted more and more attention.[31−39] Recently, we have developed a new computational approach to modeling enzyme-catalyzed reactions.[30] This approach involves a combined ab initio quantum mechanical/molecular mechanical (QM/MM) method, an iterative energy minimization procedure, and free energy perturbation simulations. It is based on a pseudobond model of the QM/MM interface introduced earlier by Zhang et al.,[29] and allows for a self-consistent and integrated energy expression for an entire QM/MM system with first-principle quantum mechanical methods which are necessary for accurate description of chemical reactions. Starting from the crystal structure, optimized structures of the reacting QM part inside the MM enzyme environment can be obtained along a reaction coordinate connecting the reactant and the product. The free energy profile associated with the reaction path can be determined by the free energy perturbation (FEP) method.[40]

In the current study, we address the two questions about the enolase mechanism as outlined above using our combined QM/MM and free energy simulation approach. Emphasis will be on the second question, which is yet to be answered. As far as the first question is concerned, the present study can be viewed as validations of both the methodology and the commonly believed role of electrostatic interactions in enhancing the acidity of the α-proton. We employ a theoretical approach involving first-principle quantum mechanical methods and the explicit enzyme environment. This approach is different from previous studies on the same system. To summarize, the following mechanistic issues will be discussed.

a. The pK_a mismatch between the α-proton and Lys345. In solution, the pK_a of the α-proton of PGA is about 32, while the pK_a of the lysine side chain is close to 10. To explain the rapid reaction rate of enolase,[19,41] the pK_a mismatch between the catalytic base and the α-proton must be accounted for.

b. The effects of the metal cations on the β-hydroxyl group leaving step. The leaving of the β-hydroxyl group results in the removal of a negative charge from the substrate. One may expect the metal cations to disfavor the second step because of their strong electrostatic interactions with the substrate. This needs to be verified.

c. The effects of the rest of the enzyme environment and how they are related to the three-dimensional structure of the enzyme. As stated above, the charge on the substrate is changing in essentially opposite directions for two reaction steps: a proton (positive) is removed from the substrate in the α-proton

(26) Zhang, E.; Brewer, J. M.; Minor, W.; Carreira, L. A.; Lebioda, L. *Biochemistry* **1997**, *36*, 12526−12534.
(27) Guthrie, J. P.; Kluger, R. *J. Am. Chem. Soc.* **1993**, *115*, 11569−11572.
(28) Alhambra, C.; Gao, J.; Corchado, J. C.; Truhlar, D. G. *J. Am. Chem. Soc.* **1999**, *121*, 2253−2258.
(29) Zhang, Y.; Lee, T.; Yang, W. *J. Chem. Phys.* **1999**, *110*, 46−54.
(30) Zhang, Y.; Liu, H.; Yang, W. *J. Chem. Phys.* **2000**, *112*, 3483−3492.
(31) Warshel, A.; Levitt, M. *J. Mol. Biol.* **1976**, *103*, 227.
(32) Singh, U. C.; Kollman, P. *J. Comput. Chem.* **1986**, *7*, 718−730.
(33) Field, M. J.; Bash, P. A.; Karplus, M. *J. Comput. Chem.* **1990**, *11*, 700−733.
(34) Gao, J. Methods and applications of combined quantum mechanical and molecular mechanical potentials. In *Review in Computational Chemistry*; VCH: New York, 1995; Vol. 7.
(35) Aqvist, J.; Warshel, A. *Chem. Rev.* **1993**, *93*, 2523−2544.
(36) Liu, H.; Muller-Plathe, F.; van Gunsteren, W. F. *J. Mol. Biol.* **1996**, *261*, 454−469.
(37) Bash, P. A.; Ho, L. L.; Mackerell, A. D., Jr.; Levine, D.; Hallstrom, P. *Proc. Natl. Acad. Sci.* **1996**, *93*, 3698−3703.
(38) Stanton, R. V.; Perakyla, M.; Bakowies, D.; Kollman, P. A. *J. Am. Chem. Soc.* **1998**, *120*, 3448−3457.
(39) Lyne, P. D.; Hodoscek, M.; Karplus, M. *J. Phys. Chem. A* **1999**, *103*, 3462−3471.
(40) Zwanzig, R. W. *J. Chem. Phys.* **1954**, *22*, 1420−1426.
(41) Dinovo, E. C.; Boyer, P. D. *J. Biol. Chem.* **1971**, *246*, 4586−4593.

abstraction step, while in the β-hydroxyl group leaving step a hydroxyl group (negative) is eliminated. If the metal cations have opposite electrostatic effects on the two steps as expected, then the enzyme should provide a mechanism to counteract the effects of the metal cations in the second step. Otherwise the entire reaction would not be feasible even though the pK_a of the α-proton has been lowered sufficiently and the first step can proceed. Equally important is that such a mechanism must not interfere with the α-proton abstraction step. It is unlikely that the enzyme may fulfill the different requirements on catalysis of the two reaction steps through conformational rearrangements, given the close similarity between the X-ray structures of the enzyme−substrate and the enzyme−product complexes.[13]

The major purpose of this work is to provide insight into the structural features of enolase related to its capability to catalyze the two different reaction steps which have apparently different requirements for transition-state stabilization.

II. Materials and Methods

A. Preparing the Initial Structure. The initial structure of yeast enolase in complex with two Mg^{2+} ions and the substrate PGA was taken from the Brookhaven protein data bank (PDB ID 1one[13]). Water molecules in the crystal structure were retained. The active site was solvated using a sphere of water centered around carbon-2 of PGA. The radius of the water sphere is 24 Å. Water molecules overlapping with atoms in the crystal structure were removed from the sphere. With a sphere of water we were using a finite system to model a system in solution. To minimize the effects of the unrealistic boundaries, we ignored conformational fluctuations of atoms far away from the active site in the subsequent calculations: we keep atoms more than 20 Å away from carbon-2 of PGA frozen.

B. Exploring the Protonation States of Titratable Groups. Based on available experimental data and the three-dimensional structure, we assigned the protonation states for most of the titratable groups of the system as described below. For His159, His373, Glu168, and Glu211, their most probable protonation states in the active species were explored using molecular dynamics (MD) simulations.

Yeast enolase has 11 histidine residues, with three of them, His132, His237, and His431, in the interior of the protein and two, His159 and His373, at the active site. On the basis of their environment, we assume that the side chain of His237 and His431 is charged, and His132 is neutral and protonated at $N_{\epsilon 2}$. The exposed histidine side chains were assumed to be neutral. The side chain of Lys345 was also assumed to be neutral. Except for the above residues, all other acidic or basic side chains were assumed to be charged. The entire system is neutral without adding any counterions.

The following energy minimization and MD simulation procedure has been used to explore the protonation states of the active site groups. For each selected combination of protonation states, the system is first optimized until the root-mean-square (RMS) energy gradient is below 1.0 kcal mol^{-1} Å^{-1}. In this step, the positions of atoms present in the crystal structure were restrained by harmonic potential energy functions with a force constant of 20 kcal mol^{-1} Å^{-2}. Then a 13 ps MD simulation is carried out. In the first 3 ps, atoms present in the crystal structure were restrained. The restraints were removed in the following 10 ps simulation.

A total number of 10 different combinations of protonation states have been simulated. All selected combinations have only one of Glu168, Glu211, and His373 protonated, and either His159 or the phosphate group of PGA protonated. The structures of the active site after the 13 ps MD simulations were examined and compared to the crystal structure. We used the following criteria to choose the active combination: the catalytic base (Lys345) and acid (one of Glu168, Glu211, or His373) should be in correct orientation to take part in the reaction; the metal ions should maintain their coordinated partners, and the hydrogen bonds between PGA and its surroundings should be maintained. For only one combination, in which Glu211 and His159 are protonated and Glu168, His373, and the phosphate group are unprotonated, have these criteria been met and the structure of the active site after the MD simulation closely approximates that in the crystal structure (see Figure 1). The active species was chosen to have this combination of protonation states, and accordingly, Glu211 was chosen as the catalytic acid.

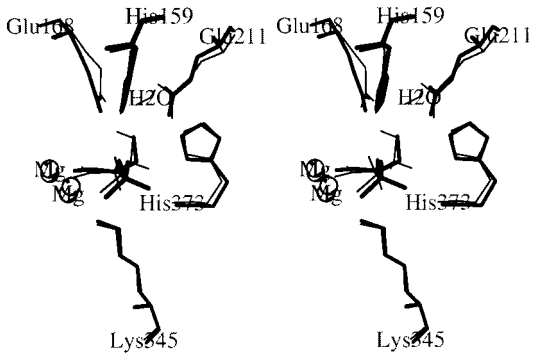

Figure 1. A comparison of the structures of the active species before (crystal structure) and after the molecular dynamics simulations. Stereoviews are shown with the crystal structure as thicker lines. Hydrogen atoms on amino acid residues have been omitted.

C. The QM/MM Potential Energy Function and QM/MM Model. A detailed account of the ab initio QM/MM potential energy function we used in this study has been given elsewhere.[29,30] Here we only give a brief description. The system is partitioned into a QM and a MM subsystem. The total energy of the system is

$$E_{\text{total}} = E_{\text{MM}} + E_{\text{QM}} + E_{\text{QM/MM}} \quad (1)$$

The QM/MM interaction energy $E_{\text{QM/MM}}$ includes bonded terms and nonbonded interactions. For the nonbonded interactions, the MM subsystem interacts with the QM subsystem as a collection of Lennard-Jones particles and point charges. When the electronic structure of the QM subsystem is determined, the charges in the MM subsystem are included in an effective Hamiltonian that describes the QM subsystem. When geometry optimization or molecular dynamics simulation is carried out on the MM subsystem, the QM/MM electrostatic interactions are approximated with fixed point charges on the QM atoms which are fitted to reproduce the electrostatic potential (ESP) of the QM part.[42] This has been shown to be a good approximation that leads to convergence of an iterative QM/MM optimization procedure (see below).[30] A key element in this QM/MM approach is the pseudobond model for the bonded QM/MM interface.[29] This model leads to a smooth connection between the QM and MM subsystems and an integrated expression for the total potential energy of the entire system.[29]

On the basis of the proposed mechanism of enolase, we partitioned the system into a QM subsystem of 44 atoms and a MM subsystem of 9281 atoms. The QM subsystem consists of the side chains of Lys345 and Glu211, the substrate PGA, and the two Mg^{2+} ions. At the bonded QM/MM interface, we used the pseudobond model. The $C_\alpha-C_\beta$ bonds of Lys345 and Glu211 were treated as the pseudobonds.

D. Determining the Reaction Paths. Ideally, one would use statistical mechanics sampling of the entire potential energy surface to determine the free energy profile along a given reaction coordinate. This is yet prohibitively costly with ab initio QM/MM methods because of the computational expenses. The majority of QM/MM studies of enzyme systems published so far are based on semiempirical QM models, some of them using statistical mechanics sampling of the entire QM/MM system. Proper statistical mechanical sampling of the QM subsystem using ab initio QM/MM models remains a challenge. Currently, the best we can afford is to use only one or a few QM structures at each point of the reaction coordinates (reaction paths) while sampling the MM subsystem extensively. Determining the reaction paths as global minimum energy paths is also out of question for such high dimensional systems. Only local minima can be reached. At first sight this may cause doubt because of the existence of many local

(42) Besler, B. H.; Merz, K. M., Jr.; Kollman, P. A. *J. Comput. Chem.* **1990**, *11*, 431−439.

minima. However, the calculated energy barriers associated with the reaction paths determined as described below, as in many other QM/MM studies of enzyme reactions, should be an upper bound of the actual barrier. That is, given the QM/MM model, the actual barrier is not expected to be higher than the calculated barrier. As long as the QM/MM potential energy function is valid and the calculated barrier is consistent with experimental reaction rate, the structure and energetics of the QM subsystem, which has much less degrees of freedom and is less flexible than the MM subsystem, must be a close approximation to the actual reaction path or be representative of the ensemble of the QM subsystem fluctuations during the reaction.

A detailed description of how a reaction path can be determined in an enzyme environment has been given elsewhere.[30] We only outline the procedure here. For each proposed reaction step, first, a reaction coordinate is chosen. Then restrained optimization of both the QM and the MM parts is performed to generate a reaction path along the reaction coordinate. The path consists of a series of representative structures of the QM part which connect the reactant to the product.

We have used two different restrained optimization procedures to generate the reaction paths for the two steps in the enolase-catalyzed reaction.

a. The Iterative Minimization Procedure. For the first reaction step, the α-proton abstraction, an iterative minimization procedure as described by Zhang et al.,[30] was used. Each iteration consists of one complete optimization of only the MM subsystem followed by another complete optimization of only the QM subsystem. In each optimization, the QM/MM interactions are always included, and the subsystem not being optimized is fixed at the geometry obtained from the previous optimization. When the MM subsystem is optimized, the charges on the QM subsystem are also fixed to the ESP charges fitting to the QM wave function resulting from the previous QM optimization. The iterations are continued until the geometries of both subsystems no longer change. The procedure is applied repeatedly with the reaction coordinate restrained at a selected set of values starting from the reactant and ending at the product.

Technically, because the MM subsystem contains a large number of degrees of freedom, only local minima can be identified through optimizations. The iterative procedure leads to meaningful total potential energies along the reaction path only if the optimizations of the MM subsystem at different reaction coordinate values do not lead to large fluctuations of the MM energy. The calculated fluctuations of the MM energies are not necessarily relevant to the reaction process if the MM part samples different local minima along the reaction coordinate. For the α-proton abstraction step, the iterative optimization indeed gave a smooth total potential energy surface of the entire QM/MM system.

b. The Energy Minimization/MD Simulation Procedure. The second step of the enolase reaction involves the dissociation of the β-hydroxyl group from the substrate. *We found that the rearrangements of the MM subsystem along the reaction coordinates cannot be captured by energy minimization.* The calculated total potential energies do not form a smooth curve along the reaction coordinate when the iterative minimization procedure is used. To model the MM rearrangements properly, we used MD simulations to relax the structure of the MM subsystem along the reaction coordinate. As in the iterative procedure, the reaction coordinate is restrained to a series of values. First, when the reaction coordinate value is changed, the QM subsystem is optimized, with the MM subsystem not yet relaxed. Then a MD simulation is carried out on the MM subsystem to accommodate the changes in the QM subsystem. During the simulation, the QM subsystem has fixed charges and geometry as obtained from the optimization of the QM subsystem. The resulting MM subsystem is further optimized by energy minimization. Finally the QM subsystem is optimized again inside the relaxed MM environment. The final geometry of the QM subsystem is used in later MD simulations of the MM subsystem. Although this procedure generates a locally optimized conformation of the MM part for each reaction coordinate value, the calculated variations of the total MM potential energy along the reaction coordinate are not necessarily relevant to the reaction process. This does not pose any difficulty for the subsequent free energy calculations, although a locally minimized total potential energy reaction path is no longer available. The reasons are the following: first, the changes in the structures and energies of the QM part still likely correspond to the reaction process; and second, the fluctuations of the MM part are to be dealt with by the free energy simulations and the total potential energies replaced by free energies.

The procedures described above are not the only means to determine the reaction paths. For example, the energy minimization/MD simulation procedure can be extended so that at each coordinate value, the procedure is carried out iteratively (simulated annealing), with a much higher computational cost. No matter what the procedure is, only local minima of the entire QM/MM energy surface can be reached, the validity and representativeness of the QM structures and energetics remain to be judged based on the upper bound argument. For the enolase reaction, the above procedures are sufficient to give continuous energy/free energy profiles along the reaction coordinate and the calculated barriers are comparable to experimental reaction rate.

We have chosen the reaction coordinate for the α-proton abstraction step (R_{c1}) to be the difference between two distances: the distance from the α-proton to carbon-2 of PGA (the proton donor) and the distance from the α-proton to N_ξ of Lys345 (the proton acceptor). The reaction coordinate for the β-hydroxyl group leaving step (R_{c2}) has been chosen as the difference between the distance from the oxygen of the β-hydroxyl group to carbon-3 of PGA and the distance from the same oxygen to the proton on the carboxyl group of Glu211 (the catalytic acid). For the α-proton abstraction step, the iterative optimization procedure was applied to determine the reaction path. For the β-hydroxyl group leaving step, the combined energy minimization/MD simulation procedure was applied to obtain the reaction path. The MD simulation for determining the reaction path at each new reaction coordinate value lasted 2 ps.

E. Determining the Free Energy Profiles. The free energy perturbation (FEP) method[40] was used to determine the free energy profiles associated with the reaction paths determined above. The relative free energies for the "solvation" or "embedding" of the reacting QM part in the enzyme environment were computed via MD simulations. These relative free energies were then combined with the QM energies of the reacting QM subsystem to obtain approximate overall free energy profiles associated with the reaction steps. We emphasize that the structures and energies of the QM subsystem have been obtained in an explicit enzyme environment with first-principle quantum mechanical methods. The major approximation involved in the resulting free energy profiles is the neglect of the free energy changes associated with fluctuations of the QM subsystem around the optimized reaction paths.[30]

The FEP calculations were carried out in the following manner. In each MD simulation, the QM subsystem is fixed to one particular "state" along the reaction coordinate. At such a state, the reaction coordinate has a particular value, and the QM subsystem has a fixed geometry and charge distribution as obtained from the reaction path calculations. This state of the QM subsystem will be called a simulated state. The free energy changes associated with perturbing the QM subsystem from the simulated state "forward" and "backward" to neighboring states along the reaction coordinate were calculated with the FEP theory.[40] The simulated states have been chosen so that for each pair of neighboring simulated states, the difference between the "forward" and "backward" FEP results is acceptably small. For the α-proton abstraction step, the reaction coordinate values (in Å) of the simulated states are $R_{c1} = -1.03$ (reactant), 0.2, 0.6, 0.8, 1.0, 1.4, and 1.7 (enolic intermediate), respectively. For the β-hydroxyl group leaving step, the reaction coordinate values (in Å) of the simulated states are $R_{c2} = 0.08$ (enolic intermediate), 0.3, 0.7, 1.0, 1.4, and 1.9, respectively. Each simulated state was equilibrated for 10 ps and sampled for 50 ps. The final relative free energies were taken as the averages of the "forward" and "backward" perturbation results.

F. Other Computational Details. Our calculations were carried out using modified versions of the Gaussian98[43] and the TINKER programs.[44] The AMBER all-atom force field parameters[45] and the TIP3P model for water[46] were used. For the QM subsystem, geometry optimizations have been carried out at the HF/3-21G level of theory with interactions with the MM subsystem treated by the QM/MM method (the HF/3-21G QM/MM model). Single-point calculations using the HF/6-31G(d) model and the density functional theory B3LYP/6-31G(d) model[47,48] have been carried out on the HF/3-21G QM/MM

geometries with interactions with the MM subsystem treated by the QM/MM method (the HF/6-31G(d)//HF/3-21G QM/MM and B3LYP/6-31G(d)//HF/3-21G QM/MM models). The QM potential energy profiles of each model are determined as the effective energies from the QM calculations minus the classical electrostatic interaction energies between the QM and MM subsystems. For calculations of the classical QM/MM electrostatics interaction energies at each reaction coordinate value, the QM charges are fitted to the QM/MM calculation on the single finally minimized QM/MM configuration. The QM energies for the HF/3-21G and HF/6-31G(d)//HF/3-21G QM/MM models, if reported, have been calculated using QM charges separately fitted to the QM/MM calculations at the corresponding levels of theory. The free energy simulations have been carried out with the charges on the QM atoms fitted to the B3LYP/6-31G(d)//HF/3-21G QM/MM calculations. For the QM subsystem, criteria for geometry optimizations are the defaults in Gaussian98. For the MM subsystem, the criterion is the root-mean-square (RMS) energy gradient being less than 0.1 kcal mol^{-1} $Å^{-1}$. In the MM minimizations, the radius of the active sphere (the sphere within which atoms were allowed to move) is 20 Å. The cutoff distance for nonbonded interactions is 15 Å. In the MD simulations, the radius of the active sphere is 22 Å. The positions of atoms in a shell from 18 to 22 Å have been restrained by a harmonic potential. A twin range cutoff method was used to treat the nonbonded interactions,[49] with a long-range cutoff of 15 Å, a short-range cutoff of 8 Å, and the nonbonded pair list updated every 20 steps. The temperature of the simulations was maintained at 300 K using the weak coupling method with a coupling time of 0.1 ps.[50] For free energy simulations, the time step used is 1 fs, and only bond lengths involving hydrogen atoms were constrained using SHAKE.[51] For the other simulations not involving free energy calculations, the time step is 2.0 fs, and all bond lengths were constrained.

III. Results and Discussions

A. Structure of the Active Species. With the chosen protonation states for the titratable groups, the active site of the relaxed active enzyme−substrate complex maintains key features of the crystal structure (Figure 1). The side chain of Lys345 is at a position ready to capture the α-proton of PGA. Glu211 is protonated and hydrogen bonded to the β-hydroxyl group of PGA, ready to act as a catalytic acid in the second step of the reaction. The β-hydroxyl group is hydrogen bonded to the unprotonated Glu168. The side chain of His373 is neutral, with its $N_{\epsilon 2}$ protonated and hydrogen bonded to a water molecule, which is in turn hydrogen bonded to the $O_{\epsilon 2}$ atoms of Glu168 and Glu211. The side chain of His159 is charged and hydrogen bonded to the phosphate group of PGA. The simulation supports the assumption that Glu211 is protonated and acts as the catalytic acid in the β-hydroxyl group leaving step, consistent with site-directed mutegenesis experiments.[23] The simulation also supports that the phosphate group of PGA is not protonated by His159, consistent with recent pH dependence experimental studies.[20]

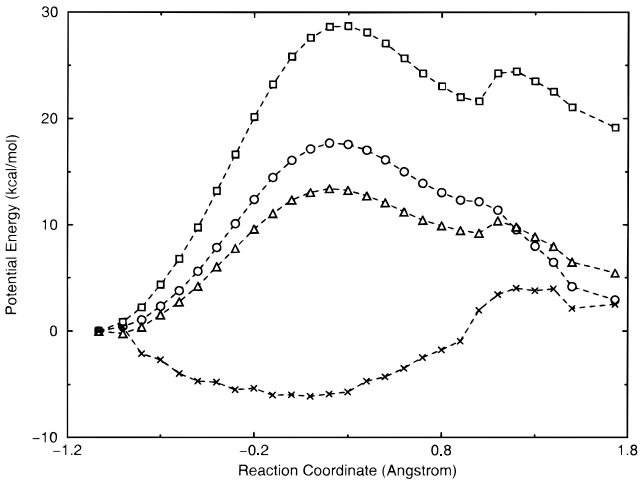

Figure 2. Relative total potential energy surfaces of the α-proton abstraction step calculated at different levels of theory: HF/3-21G QM/MM (○), HF/6-31G(d)//HF/3-21G QM/MM (□), and B3LYP/6-31G(d)//HF/3-21G QM/MM (△). The contribution from the MM part ($E_{MM} + E_{QM/MM}$) for the B3LYP/6-31G(d)//HF/3-21G QM/MM model is also shown (×).

B. Energy and Free Energy Surfaces of the α-Proton Abstraction Step. For this step, the total potential energy surfaces of the entire QM/MM system along the reaction path were obtained. The potential energy surfaces calculated with various models are shown in Figure 2. The transition state is around $R_{c1} = 0.2$ Å. The barrier heights are 17.6, 28.5, and 13.3 kcal mol^{-1} from the HF/3-21G, HF/6-31G(d)//HF/3-21G, and B3LYP/6-31G(d)//HF/3-21G QM/MM calculations, respectively. On the HF/3-21G QM/MM surface, there is a shoulder around $R_{c1} = 0.9$ to 1.0 Å, which turns into a marginly stable intermediate on the B3LYP/6-31G(d)//HF/3-21G and HF/6-31G(d)//HF/3-21G QM/MM surfaces. This shoulder is associated with a local conformational change after the proton transfer, a rotation of the amino group of Lys345 around the $C_\delta - N_\zeta$ bond. The rotation results in two hydrogen bonds between Lys345 and the enolic intermediate. One hydrogen bond involves the phosphate and the other involves the carboxylate group. The driving force for this conformational change can be the enhanced electrostatic interactions between Lys345 and the negative charges of the enolic intermediate.

The approximate free energy surface obtained by combining the QM part of the potential energy (B3LYP/6-31G(d)//HF/3-21G QM/MM model) and the free energy perturbation calculations is shown in Figure 3. The overall free energy surface is essentially the same as the total potential energy surface, suggesting that the fluctuations of the MM part play a minor role in this step. Figure 3 also shows that the differences between the forward and backward free energy results are small, indicating convergence of the simulations. The calculated free energy barrier is 13.1 kcal mol^{-1} within the B3LYP/6-31G(d)//HF/3-21G QM/MM model.

(43) Frisch, M. J.; Trucks, G. W.; Schlegel, H. B.; Scuseria, G. E.; Robb, M. A.; Cheeseman, J. R.; Zakrzewski, V. G.; Montgomery, J. A., Jr.; Stratmann, R. E.; Burant, J. C.; Dapprich, S.; Millam, J. M.; Daniels, A. D.; Kudin, K. N.; Strain, M. C.; Farkas, O.; Tomasi, J.; Barone, V.; Cossi, M.; Cammi, R.; Mennucci, B.; Pomelli, C.; Adamo, C.; Clifford, S.; Ochterski, J.; Petersson, G. A.; Ayala, P. Y.; Cui, Q.; Morokuma, K.; Malick, D. K.; Rabuck, A. D.; Raghavachari, K.; Foresman, J. B.; Cioslowski, J.; Ortiz, J. V.; Stefanov, B. B.; Liu, G.; Liashenko, A.; Piskorz, P.; Komaromi, I.; Gomperts, R.; Martin, R. L.; Fox, D. J.; Keith, T.; Al-Laham, M. A.; Peng, C. Y.; Nanayakkara, A.; Gonzalez, C.; Challacombe, M.; Gill, P. M. W.; Johnson, B. G.; Chen, W.; Wong, M. W.; Andres, J. L.; Head-Gordon, M.; Replogle, E. S.; Pople, J. A. *Gaussian 98*, Revision A.5; Gaussian, Inc.: Pittsburgh, PA, 1998).

(44) Ponder, J. W. *TINKER, Software Tools for Molecular Design, Version 3.6*; The most updated version for the TINKER program can be obtained from J. W. Ponder's World Wide Web site at http://dasher.wustl.edu/tinker., June 1998.

(45) Cornell, W. D.; Cieplak, P.; Bayly, C. I.; Gould, I. R.; Merz, K. M.; Ferguson, D. M.; Spellmeyer, D. C.; Fox, T.; Caldwell, J. W.; Kollman, P. A. *J. Am. Chem. Soc.* **1995**, *117*, 5179−5197.

(46) Jorgensen, W. L.; Chandrasekhar, J.; Madura, J.; Impey, R. W.; Klein, M. L. *J. Chem. Phys.* **1983**, *79*, 926−933.

(47) Becke, A. D. *J. Chem. Phys.* **1993**, *98*, 5648−5652.

(48) Lee, C.; Yang, W.; Parr, R. G. *Phys. Rev. B* **1988**, *37*, 785.

(49) van Gunsteren, W.; Berendsen, H.; Colonna, F.; Perahia, D.; Hollenberg, J.; Lellouch, D. *J. Comput. Chem.* **1984**, *5*, 272−279.

(50) Berendsen, H. J. C.; Postma, J. P. M.; van Gunstereno, W. F.; DiNola, A.; Haak, J. R. *J. Chem. Phys.* **1984**, *81*, 684−3690.

(51) Ryckaert, J.-P.; Ciccotti, G.; Berendsen, H. J. C. *J. Comput. Phys.* **1977**, *23*, 327−341.

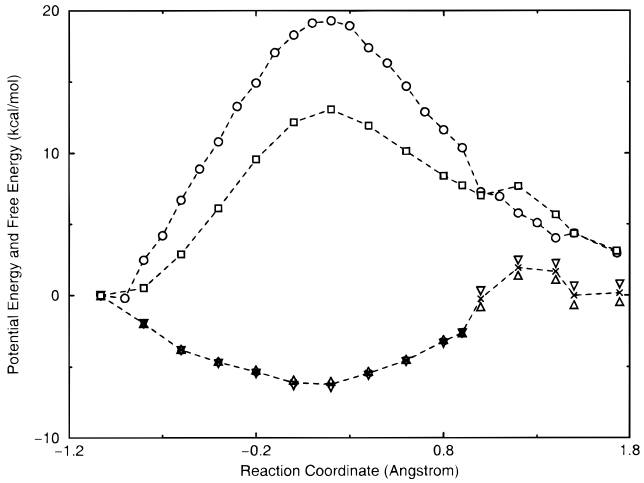

Figure 3. Relative potential energy and free energy surfaces of the α-proton abstraction step calculated with the B3LYP/6-31G(d)//HF/3-21G QM/MM model: ○, QM potential energy; ×, free energy associated with interactions with the MM part; □, total free energy surface. The forward (▽) and backward (△) free energy perturbation results are also shown.

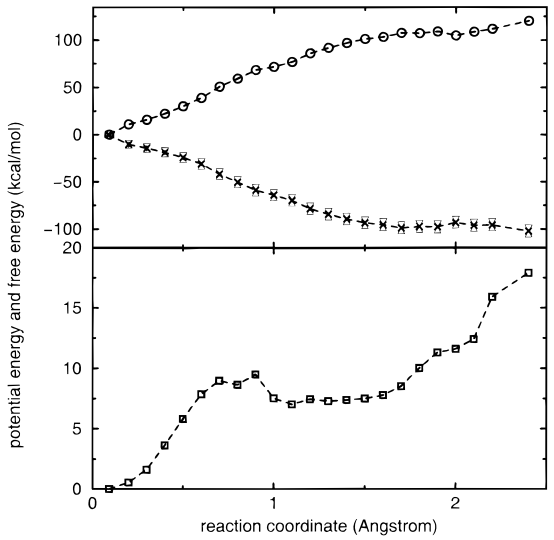

Figure 4. Relative potential and free energy surfaces of the β-hydroxyl leaving step calculated with the B3LYP/6-31G(d)//HF/3-21G QM/MM model: ○, QM potential energy; ×, free energy associated with interactions with the MM part; □, total free energy surface. The forward (▽) and backward (△) free energy perturbation results are also shown.

C. Free Energy Surface Associated with the β-Hydroxyl Group Leaving Step. For this step, the free energy surface is shown in Figure 4. As explained above, the calculated total QM/MM potential energies for this step are not relevant. The geometry of the QM part changes continuously along the reaction path, as does the QM potential energy (Figure 4). This justifies the energy minimization/MD simulation approach we used to obtain the reaction path for this reaction step.

When the change in reaction coordinate is examined closely, the initial part (from $R_{c2} = 0.08$ to 0.5 Å) of the reaction process is dominated by the proton transfer from Glu211 to the β-hydroxyl group of the enolic intermediate. The remaining part corresponds to the leaving of the protonated β-hydroxyl group (as a water molecule) from carbon-3 of the substrate. On the energy and free energy surfaces, there is no indication of any β-hydroxyl-protonated enolic intermediate. From the enolic intermediate to product is essentially a single step. The calculated forward and backward free energy surfaces for the second step also agree well, an indication of convergence of the FEP calculations. Perhaps because of the artificial restrain on the shell of atoms surrounding the active site, further dissociation of the leaving water molecule from the substrate results in an increase of the free energy of the system. To obtain a more a realistic free energy profile at larger reaction coordinate values, a more sophisticated treatment of the boundary—without any artificial position restrains—may be necessary. In this work we are interested only in the chemical reaction processes, which is most appropriate for studies using QM/MM models. Binding or releasing of the substrates is out of the scope of the current study.

From Figure 4, the barrier hight for this step is 9.4 kcal mol^{-1} with the B3LYP/6-31G(d)//HF/3-21G QM/MM model, about 4 kcal mol^{-1} lower than the barrier for the first step. Recent kinetic isotope effect experiments[19] have indicated that both the α-proton abstraction step and one or both of the β-hydroxyl group leaving or product releasing steps are kinetically significant. Earlier studies have shown that the observed primary isotope effects of the α-proton abstraction step strongly depend on pH and on cation concentration.[52] Given these observed primary isotope effects as an indicator of the rate limiting capability of the α-proton abstraction step, the results suggest that this step can be partially but not cleanly rate limiting. It has been estimated based on the rate constant[23] that the activation barrier is approximately 15 kcal mol^{-1}.[28] This estimation is very close to our calculated barrier of the proton abstraction step (13.1 kcal mol^{-1}). Our calculation is consistent with the theory that the α-proton abstraction step is kinetically significant. The kinetic significance of the hydroxyl group leaving step cannot be excluded because, first, the difference between the calculated barrier heights of the two steps is small (4 kcal mol^{-1}) and, second, the important role of the electrostatic environment in modulating the barriers, which we will discuss below, may implicate the pH dependence of the kinetic isotope effects.[52] The product releasing step is not studied in this work. Although product releasing may also be partially rate limiting, it cannot be exclusively rate determining provided that the proton abstraction is kinetically important, as suggested by both our calculations and experiments.[19]

D. Effects of the Metal Cations and the Rest of the Enzyme on the α-Proton Abstraction Step. Now we address the first mechanistic issue raised in the Introduction—how the pK_a mismatch between the α-proton and Lys345 is compensated. The major factors that lower the energy barrier associated with the α-proton abstraction by Lys345 are the two metal cations. As the two metal ions have been included in the QM subsystem, so are their contributions included in the QM part of the energy. It is technically difficult to separate out the contributions of the metal ions accurately through gas-phase calculations, because that would involve calculations on the removal of a proton from the trianionic PGA species. However, a qualitative estimation can be obtained. On the basis of the pK_a difference between the proton donor and acceptor (about 22 pK_a unit), the proton-transfer barrier without any catalyst should be higher than 30 kcal mol^{-1}. The QM potential energy surface (Figure 3) shows that with the two metal cations, the barrier hight is only 19.2 kcal mol^{-1} when calculated with the B3LYP/6-31G(d)//HF/3-21G QM/MM model (we note that this QM potential energy surface absorbs contributions from polarization of the QM electronic state by the MM environment, which is not expected to change significantly along the reaction coordinate).

(52) Shen, T. V.; Westhead, E. W. *Biochemistry* **1973**, *12*, 3333−3337.

The metal ions are not the only factors contributing to transition-state stabilization in this step. The activation barrier on the total QM/MM potential energy surface (Figure 2) is 5.9 kcal mol^{-1} lower than the QM potential energy surface (Figure 3). This lowering is caused by interactions of the entire QM subsystem with the MM subsystem. The free energy surface shows similar results (Figure 3). The interactions between the MM part and the QM part stabilize the transition state relative to the reactant by 6.2 kcal mol^{-1} in terms of free energy (Figure 3).

Thus our results are consistent with the previous proposition.[27,28] Electrostatic interactions, mainly with the metal ions and less significantly with the rest of the enzyme environment, are sufficient to lower the activation barrier of the α-deprotonation step.

E. Effects of the Metal Ions on the *β*-Hydroxyl Group Leaving Step. This section addresses the second mechanistic issue raised in the Introduction. While the overall free energy barrier is low for this step (only about 9.4 kcal mol^{-1}, Figure 4), it is a result of the sum of a large positive QM potential energy contribution (68.4 kcal mol^{-1} using the B3LYP/6-31G(d)//HF/3-21G QM/MM model) and a large negative free energy contribution from the MM environment (−58.9 kcal mol^{-1}) at the transition state (Figure 4). For larger reaction coordinate values, the QM contribution is even larger.

By definition, the metal ions have been included in the QM subsystem. A more quantitative separation of the contribution of the metal ions is not feasible using QM calculations for reasons mentioned previously. However, the large positive QM contribution to the activation free energy must in great part be attributed to the presence of the two metal cations. This is reasonable because accompanying the *β*-hydroxyl group leaving step, a unit negative charge is removed from the enolic intermediate, mostly from the carboxylate group which interacts directly with the binuclear metal center. As a result, the interactions with the metal cations are significantly weaker after the leaving of the hydroxyl group.

F. Effects of the Rest of the Enzyme on the *β*-Hydroxyl Group Leaving Step. The large destabilization effect of the metal cations is compensated for by the rest of the enzyme. The MM contribution stabilizes the transition state relative to the enolic intermediate by 58.9 kcal mol^{-1}. Without this contribution, the leaving of the *β*-hydroxyl group would be impossible even with Glu211 as the general acid catalyst, which has been included in the QM part. A model using a cluster of active site groups without the rest of the enzyme would not be able to capture these effects.

It is interesting to compare the effects of the metal ions and the rest of the enzyme (excluding the general base and general acid groups, Lys345 and Glu211, and the two metal ions) in the two reaction steps. The roles of the metal ions are straightforward to understand. When the positive proton is removed from the substrate, the metal ions favor the reaction step. When the negative hydroxyl group is removed, they disfavor the reaction step. Thus the roles of the metal cations in the second step are consistent with their roles in the first step in terms of electrostatic interactions with the substrate.

The roles of the rest of the enzyme environment are not as straightforward as those of the metal ions. Instead of having counter effects on the two steps as the metal ions, it favors both steps despite the fact that the charge on the substrate changes oppositely. It stabilizes the transition states of both reaction steps, modestly for the first step but most significantly for the second step.

Scheme 2

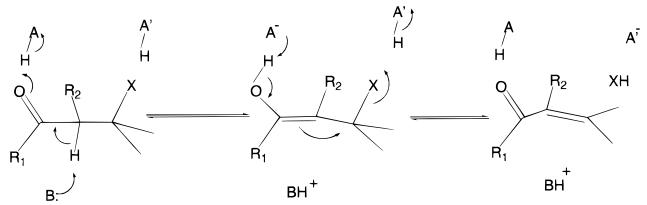

It is interesting to compare the effects of this enzyme environment to the role of a general acid−general base catalyst in a mechanism proposed by Gerlt and Gassman some time ago (Scheme 2).[6] In Scheme 2, the group XH acts as a general acid catalyst during the removal of the α-proton. Then the resulting conjugate base X$^-$ acts as a general base during the leaving of the *β*-hydroxyl group. Energetically, the metal ions in enolase and the general acid group XH should have similar effects on the removal of the α-proton. When the second step is considered, the metal ions cannot play the same role as the conjugate base X$^-$. Actually, the effects of the metal ions on the second step are opposite to those of X$^-$. In this sense, the combination of the metal cations and the rest of the enzyme seems to have analogous energetic effects as the proposed catalysts XH/X$^-$ in Scheme 2. In enolase it is the rest of the enzyme environment that has two alternating effects during the two reaction steps (in one step it favors removing a proton and in the other it favors removing a hydroxyl group) as the alternating effects of XH and X$^-$.

We focus the remaining analyses and discussions on how this alternation of effects is possible without involving any chemical processes such as the transformation between the conjugate acid and base groups or any large scale conformational rearrangement (which was not observed during the simulations). The knowledge of the structures and charge distributions of the transition states from the QM/MM calculations makes such analyses possible

G. Energy Decomposition Analyses of the Effects of Individual Residues. To understand the role of individual residues, certain decomposition of the overall effects of the MM environment is necessary. While a decomposition of the free energy barrier associated with the two reaction steps may not be possible, breaking the energy barrier into components is possible. Note that we do not use the energy components for quantitative predictions, and we only use them as qualitative indicators to facilitate our understanding of the structure−function relationship of this enzyme. The analyses can be combined with the three-dimensional structure of the enzyme to identify the structural origin of the different transition-state stabilizing effects discussed above.

We consider the changes in electrostatic interaction energies between individual residues and the QM part when the system goes from reactant (or the enolic intermediate) to transition states,

$$\Delta E_i = \langle E_{i/\mathrm{QM}}^{\mathrm{electrostatic}} \rangle_{\mathrm{MM,transition\ state}} - \langle E_{i/\mathrm{QM}}^{\mathrm{electrostatic}} \rangle_{\mathrm{MM,reactant}} \quad (2)$$

where i represents a residue (or a water molecule) in the MM part, $E_{i/\mathrm{QM}}^{\mathrm{electrostatic}}$ represents the electrostatic interaction energies between residue i and the QM part, and $\langle ... \rangle_{\mathrm{MM,reactant}}$ and $\langle ... \rangle_{\mathrm{MM,transition\ state}}$ represent averages over the ensembles where the conformational space of the MM part is sampled with the QM part corresponding to the reactant (or enolic intermediate) and the transition states, respectively. ΔE_i can only be viewed as a first-order approximation to the energetic contribution of

Table 1. Residues Contributing Significantly to Transition-State Stabilization ($|\Delta E_i| \geq 1.0$ kcal mol^{-1}) in Either the First (α-proton abstraction) or the Second (β-hydroxyl group leaving) Step of the Enolase-Catalyzed Reaction

		ΔE_i (kcal mol^{-1})[b]		
categories[a]	residues	first step	second step	region[c]
1	*Ala*38	−1.5	−1.1	I
	*Ser*39	0.9	−1.4	I
	*His*159	−5.7	−1.1	III
	*Gln*167	−4.0	0.8	I
	*Lys*396	−5.5	5.4	I
	*Arg*374	−2.5	5.2	I
2	*Glu*44	−2.2	−4.4	II
	*Asp*246	5.8	−8.6	I
	*Glu*251	0.9	−1.1	I
	*Glu*295	1.2	−6.5	I/II
	*Asp*296	0.7	−4.0	I/II
	*Glu*300	0.5	−1.3	I/II
	*Asp*320	−4.4	−12.1	II
	*Asp*321	−1.0	−4.1	I/II
	*H2O*443	0.1	−2.4	I
	*H2O*444	−0.4	−1.6	I
3	*Arg*14	−1.2	−2.6	III
	*Arg*402	−0.3	−1.7	III
	*Arg*405	−1.7	−5.8	III
	H_2O440	−0.4	−3.9	I/III
	H_2O447	−0.5	−4.8	I/III
4	*Asn*152	5.8	−8.1	III
	*Asn*155	−0.4	1.3	III
	*Glu*168	7.4	−4.6	I
	*Asp*210	3.3	2.0	III
	*His*373	−2.3	−1.9	I/II/III/IV
	*Gly*398	−0.3	−1.1	III
	*Glu*404	0.4	2.2	III
	H_2O523	1.9	−0.8	I/II
total		−8.1	−70.1	

[a] The residues in the first category are the positively charged or hydrogen bond donor residues in regions I/III. The second category includes the mostly negatively charged residues in regions I/II. The residues in the third category are those which preferentially favor the β-hydroxyl group leaving step but are not classified into the first and second categories. The fourth category includes the remaining residues. [b] The contribution of individual residue to transition-state stabilization in the two reaction steps from the energy decomposition analysis (see eq 2 in the text). [c] See Figure 6 and the text for the definition of the regions.

residue *i* to transition-state stabilization, which means that factors such as conformational change or dielectric screening are absent. Negative ΔE_i indicates that the residue lowers the barrier and positive ΔE_i indicates the opposite.

When the two reaction steps of enolase were analyzed in this manner, we found that only a few residues and water molecules contribute significantly ($|\Delta E_i| > 1.0$ kcal mol^{-1}) in either step of the reaction. These residues are listed in Table 1 and shown in Figure 5. The analyses were carried out without additional MD simulations, only using the conformations sampled by the free energy simulations. Thus ΔE_i values for the β-hydroxyl group leaving step were not calculated exactly at the transition state ($R_{c2} = 0.9$ Å), but using the simulation at $R_{c2} = 1.0$ Å. The ensemble averages were approximated by averages over 50 conformations sampled by the free energy simulations. The conformations are equally separated in simulation time (1 ps between conformations). That ΔE_i values are qualitative indicators of contributions of individual residues is justified: the sums of ΔE_i values over all residues and water molecules (−8.1 and −70.1 kcal mol^{-1} for the two reaction steps, respectively) are relatively good approximations to the FEP results (−6.2 and −63.7 kcal mol^{-1}, respectively).

H. Correlations between the Energy Decomposition Analyses and Site-Directed Mutegenesis Studies. The data in Table 1 are consistent with several site-directed mutegenesis studies on enolase.

a. Ser39 Mutant. Table 1 shows that residues Ala38, Ser39, and Glu44 contribute significantly to transition-state stabilization. In the three-dimensional structure, the side chain of Ser39 is coordinated with one of the metal ions.[16] Replacing Ser39 by Ala causes significant loss of activity.[21] It has been suggested based on experiments that in the wild-type enzyme, certain transition-state stabilizing interactions exist between the loop around residue 39 and the reacting part.[21]

b. His373 Mutant. Another residue studied by site-directed mutegenesis is His373.[22] When the contributions from His373 (Table 1) are closely examined, we found that they mainly come from the backbone of His373, which does not change upon mutation. We expect that the major role of the His373 side chain may be not to directly participate in transition-state stabilization, but to maintain the active orientations of Glu211 and Glu168 through hydrogen bonds intermediated by a water molecule. Experimentally, it was found that the V_{max} of the His373Gln mutant relative to the wild type does not change when pH changes from 8.4 to 7.6.[22] This suggests that the change in protonation states of His373 does not have significant effects on transition-state stabilization.[22]

c. Glu168 Mutant. The properties of the mutant Glu168Gln have also been reported.[23,25] It was shown that the ability of the enzyme to catalyze the exchange of the α-proton with solvent is not significantly influenced by the mutation, but the activity of the enzyme to catalyze a reaction which mimics the reverse of the β-hydroxyl group leaving step is reduced.[23] Table 1 shows that in terms of transition-state stabilization, Glu168 does not contribute favorably to catalysis in the α-proton abstraction step, but it does contribute favorably to the forward reaction of the β-hydroxyl group leaving step. In the backward reaction, we speculate that Glu168 is needed to cooperate with Glu211 to coordinate the nucleophilic water.

I. Correlations between the Energy Decomposition Analyses and the Three-Dimensional Arrangements of Amino Acid Residues. First, we partition the active site into different regions qualitatively according to the charge redistribution processes. Consider the charge redistributions of the QM part in the two reaction steps. Accompanying the α-proton abstraction step, positive charge accumulates on Lys345 while negative charge on carbon-2 and the carboxylate group of PGA. A plane can be approximately defined according to the position and direction of this charge reorganization process. This plane (plane 1 in Figure 6) would separate PGA from Lys345 as well as approximately partition the active site into two parts: the part on the PGA side (regions I and III in Figure 6) and the part on the Lys345 side of the plane (regions II and IV in Figure 6).

In the β-hydroxyl group leaving step, the charge rearrangement takes place in a different direction: negative charge on the carboxylate group of PGA decreases and goes to Glu211. A second plane can be defined approximately according to the position and direction of this charge reorganization process (plane 2 in Figure 6). This plane separates Glu168 from Glu211 and partitions the active site into two halves with the first consisting of regions I and II and the second of regions III and IV in Figure 6.

Second, it can be expected that the contributions of individual groups to the two steps are qualitatively determined by their charge distributions and the regions they belong to. Regions I/III and II/IV are separated by plane 1, which is associated

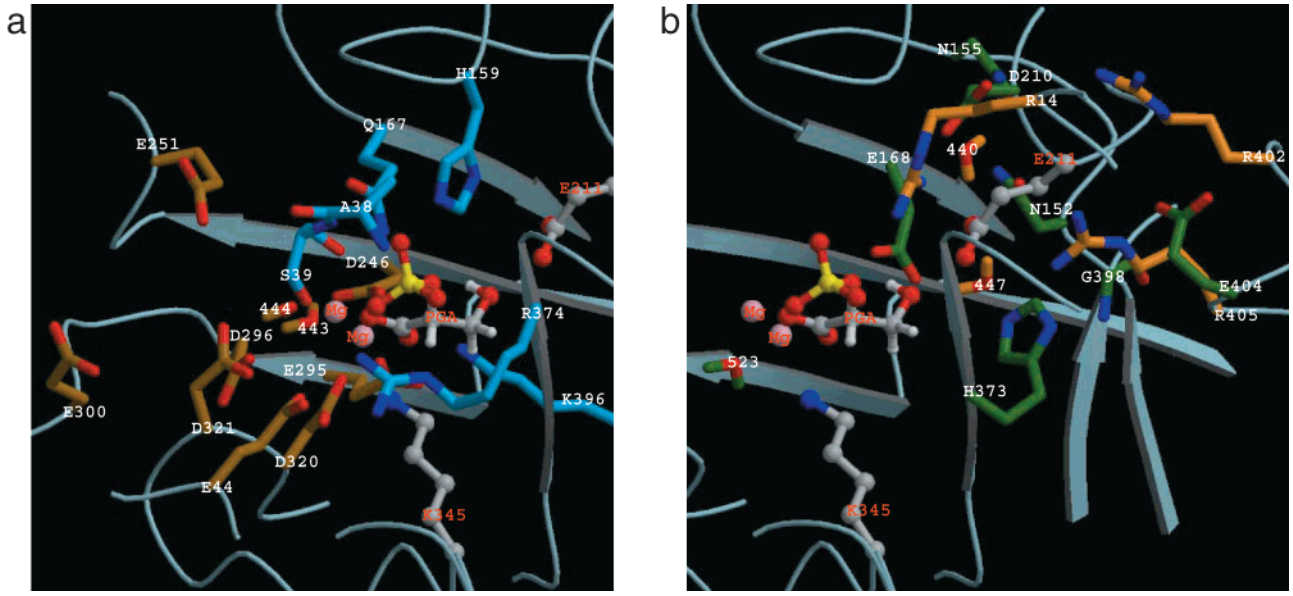

Figure 5. Catalytically important residues and water molecules at the active site of enolase. In parts a and b, the orientations of the molecular system are the same, but the view port is shifted to the right from a to b. In part a, the two metal cations are near the center, the substrate is to the left of the metal ions, Lys345 is below the substrate, and Glu211 is to the upper right of the substrate. These groups are shown as balls and sticks. The groups listed in Table 1 are shown as sticks. Oxygen atoms are in red, nitrogen atoms are in dark blue. Carbon and hydrogen atoms are in distinctive colors according to their membership in the four categories discussed in the text and listed in Table 1. For clarity, part a only shows groups in categories 1 (sky blue) and 2 (dark golden), and b only shows groups in categories 3 (green) and 4 (orange). Hydrogen atoms of amino acid residues are omitted.

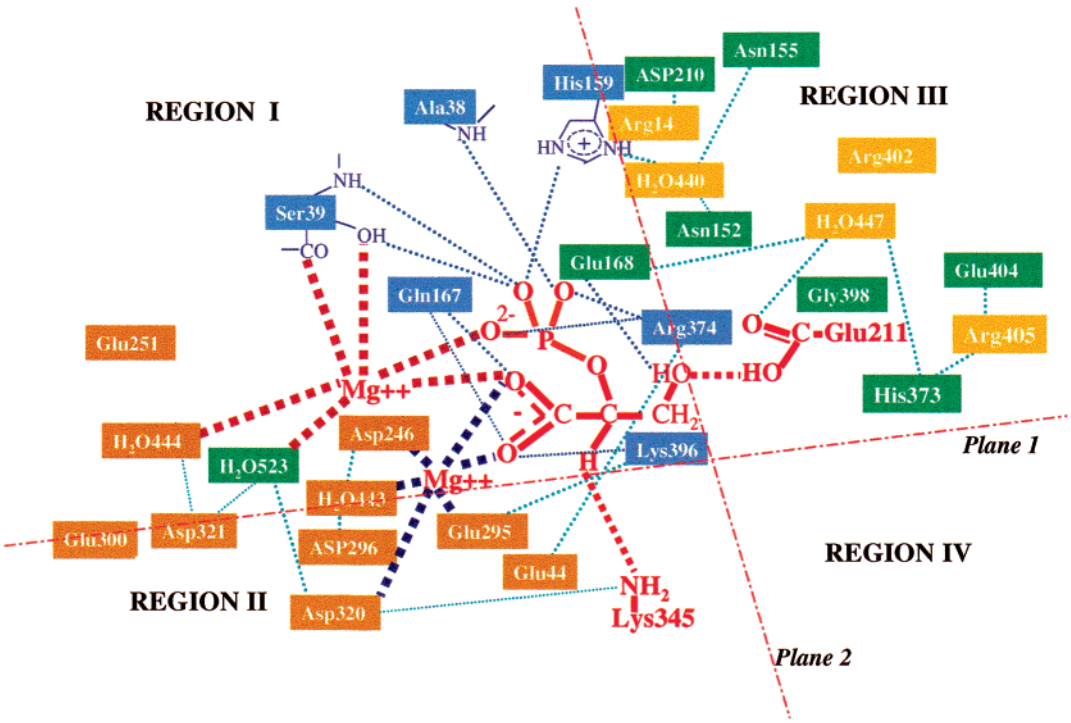

Figure 6. Positions of energetically important amino acid residues and water molecules relative to the reacting part of the enzyme system. Plane 1 is approximately defined to be perpendicular to the charge redistribution direction during the proton transfer from the substrate PGA to Lys345. It bisects PGA and Lys345. Plane 2 is approximately defined to be perpendicular to the charge redistribution direction during the β-hydroxyl group leaving assisted by Glu211. It bisects Glu211 and the carboxylate end of the substrate. Coordination of the metal ions is shown as thicker dashed lines, and hydrogen bonds are shown as dashed lines. Groups in different categories according to our discussions have different colors: category 1 in blue, category 2 in dark gold, category 3 in orange, and category 4 in green.

with the first step. Negatively charged groups in regions I and III would disfavor while positively charged groups would favor the α-proton abstraction effects. In regions II and IV, the effects would be the opposite. Regions I/II and III/IV are separated by plane 2, which is associated with the β-hydroxyl group leaving step. Residues in regions I/II would have opposite effects on the second step when compared with residues in regions III/IV.

Third, the above considerations explain the results of the energy decomposition analyses. Table 1 lists the contributions of catalytically important residues and water molecules estimated

from the energy decomposition analyses and the geometric regions they belong to. Figure 5 shows the three-dimensional arrangement of these groups relative to the reacting part in the active site. The schematic Figure 6 shows an approximate two-dimensional projection of the positions of these groups relative to the two planes associated with the charge reorganization procedures.

Now we discuss the correlation between the energy decomposition results and the position of each residue relative to the two geometric planes. With the focus on understanding how these residues significantly stabilize the transition state of the second step without destabilizing the transition state of the first step, we discuss them in four categories (see below). Residues in the first category are mainly responsible for the modest transition-state stabilization of the α-proton abstraction step. Residues in the second and third categories are responsible for the large transition-state stabilizing effects on the *β*-hydroxyl group leaving step. The remaining ones are classified into the fourth category for completeness.

Category 1: Residues in Regions I/III and Forming Hydrogen Bonds with the Substrate. Lys396 and Gln167 form hydrogen bonds with the carboxylate group of PGA, and His159, Arg374, and the backbone group of Ala38 interact with the phosphate group (Figure 5a).

These residues belongs to regions I/III (Figure 6) and have large transition-state stabilizing effects on the α-proton abstraction step. The backbone NH group of Ser39 in region I is also hydrogen bonded to the phosphate group, but its dipole moment is approximately parallel to plane 1. Its backbone CO group points to plane 1 and side chain OH group is coordinated with one of the metal ions.

When the *β*-hydroxyl group leaving step is considered, the roles of these residues vary. The positively charged Lys396 and Arg374 in region I have large transition-state destabilizing effects, consistent with their positions relative plane 2. His159 has smaller effects on this step because it is close to the interface between region I and III. Gln167 in region I also has smaller effects because its dipole moment points toward the carboxylate group of PGA, approximately parallel to plane 2. The dipole moments of the CO group of Ala38 and NH group of Ser39 in region I point toward plane 2 and thus stabilize the transition state.

Category 2: Residues Near the Interface between Region I and II of the Active Site. A number of negatively charged residues, including Glu44, Asp246, Glu295, Asp296, Glu300, Asp320, and Asp321, are crowded near plane 1, at the interface between regions I and II (Figures 5a and 6). For some of them, it is difficult to define whether they should belong to region I or region II.

Because these residues are close to plane 1, they should not affect the charge reorganizations across plane 1. Table 1 shows that they have relatively small effects on the α-proton abstraction step. Only two of them have well-defined positions relative to plane 1: Asp246 is in region I and has strong transition-state destabilizing effects, while Asp320 is in region II and has strong transition-state stabilizing effects. The sum of the contributions of all these negatively charged residues at this corner of the active site to the α-proton abstraction step is very small (0.55 kcal mol^{-1}).

When the *β*-hydroxyl group leaving step is considered, the same group of residues contributes significantly to transition-state stabilization. From Table 1, the sum of their contributions is −40.9 kcal mol^{-1}. This is because they are all on the same side of plane 2, and charge reorganizations across plane 2 should change their interactions with the reacting part significantly.

Also in region I and near region II, there are two water molecules (water 443 and 444 in Table 1) coordinated with the metal ions. They contribute relatively little to the α-proton abstraction step because their dipole moments are approximately parallel to plane 1. Their contributions to the *β*-hydroxyl group leaving step are much larger because their dipole moments point away from plane 2.

Category 3: Other Residues Having Large Transition-State Stabilizing Effects on the β-Hydroxyl Group Leaving Step but Smaller Effects on the α-Proton Abstraction Step. These include Arg14, Arg402, and Arg405, and two water molecules (waters 440 and 447 in Table 1) in region III (Figures 5b and 6). As expected from their positions, the positively charged arginine residues have transition-state stabilizing effects on both reaction steps. However, their effects on the *β*-hydroxyl group leaving step are much larger than those on the α-proton abstraction step. The large effects of waters 440 and 447 on the second step are probably results of their direct interactions with Glu211 and the leaving hydroxyl group.

Category 4: Other Residues. Negatively charged Glu168 in region I and Asp210 in region III both have large transition-state destabilizing effects on the α-proton abstraction step, while Glu168 favors and Asp210 disfavors the leaving of the *β*-hydroxyl group. Asn152 in region III also has strong transition state stabilizing effects on the *β*-hydroxyl group leaving step because of its strong interactions with Glu211 and the leaving hydroxyl group. However, it also has strong transition-state destabilizing effects on the α-proton abstraction step. Asn155 is also in region III. It disfavors the *β*-hydroxyl group leaving step but has small effects on the α-proton abstraction step. Water 523 is at the interface between regions I and II, its dipole moment disfavors the α-proton abstraction step but has small transition-state stabilizing effects on the *β*-hydroxyl group leaving step. The effects of Gly398 come from its backbone groups (Figures 5b and 6).

Finally, we can address the last mechanistic issue raised in the Introduction. The majority of the residues in Table 1 fall in the first three categories. The first and second category of residues form a distinct structural feature of the active site of enolase: mostly positive or hydrogen bond donor residues in regions I/III (the first category) and mostly negative residues in regions I/II (the second category). This structure feature seems to play a key role in dictating the electrostatic effects of the enzyme environment on the two reaction steps. Not only does the charge on the substrate change oppositely during the two reaction steps, but also the charge reorganization procedures take place in different directions in space (planes 1 and 2 are approximately perpendicular to each other). The structure of the enolase active site takes advantage of this difference. Residues in the first category modestly lower the barrier of the first reaction step by electrostatically stabilizing the developing negative charge on the substrate. They do not have significant influence on the second step. Residues in the second category significantly favor the leaving of the hydroxyl group, thus compensating for the transition-state destabilizing effects of the metal ions. They do not have large effects on the transfer of the α-proton from the substrate to Lys345 during the first step. We summarize the results in Figure 7, which emphasizes that besides the obvious catalytic groups such as the metal cations and the general acid/base groups, the enzyme environment is an essential part of the reaction mechanism.

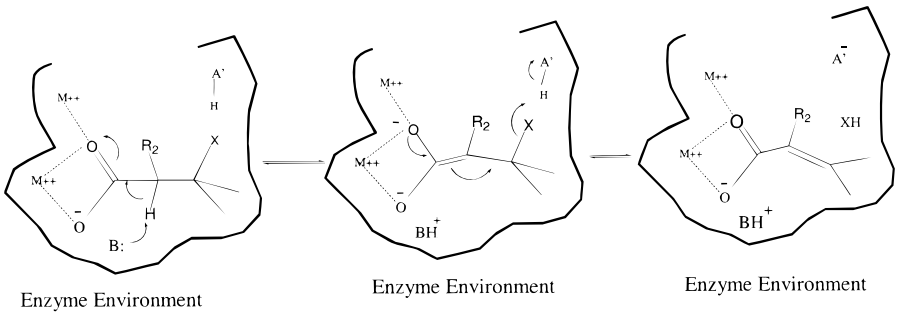

Figure 7. In the presence of the two metal cations, a reaction scheme leaving out the enzyme environment does not hold. The enzyme environment is an essential part of the mechanism just as the cations and the general acid/base groups are. While the metal cations favor the abstraction of the α-proton by the general base B, they strongly disfavor the leaving of the β group X. The enzyme environment counter balances the effects of the metal cations in the second step without interfering with the first step.

IV. Conclusions

We have studied the reaction catalyzed by enolase using a combined ab initio quantum mechanical and molecular mechanical approach recently developed in our laboratory. The free energy barriers associated with the two reaction steps of this reaction were determined. The calculated activation barriers for the two steps are 13.1 and 9.4 kcal mol^{-1}, respectively, with combined B3LYP/6-31G(d)//HF/3-21G QM/MM models. The barrier heights are comparable to estimations[28] (approximately 15 kcal mol^{-1}) based on the experimental reaction rate constant.[23] They are also consistent with experimental suggestions that the deprotonation step is partially but not exclusively rate limiting.[19] Our results confirm the previous proposition that the deprotonation by Lys345 is mainly favored by the two divalent metal ions. However, the same metal ions strongly disfavor the second step because the leaving β-hydroxyl group takes away unit negative charge from the substrate. Besides Glu211 as a general acid catalyst in the second step, the electrostatic environment plays a key role: it compensates for the disfavoring effects of the metal cations.

To understand how the enzyme environment can favor two reaction steps which result in opposite changes of charge on the substrate, we carried out energy decomposition analyses of the activation barriers of the two reaction steps. The analyses are well correlated with available site-directed mutegenesis studies on enolase. More importantly, combining the three-dimensional structure of the active site and the theoretical results (especially the analyses on the roles of individual residues in transition-state stabilization) brought about an important insight into the structure−function relationship of this enzyme. That is, the polar and charged residues at the active site are organized in a distinctive manner so that they do not interfere with (only modestly enhance) the transition-state stabilizing effects of the metal cations in the α-proton abstraction step. At the same time, they effectively compensate for the transition-state destabilizing effects of the same metal cations in the β-hydroxyl group leaving step.

The organization of the active site takes advantage of the fact that the charge reorganization procedures accompanying the two reaction steps take place in two directions which are almost perpendicular to each other. Thus a group of charged/polar residues can strongly influence the charge reorganization in one direction without interfering with the charge reorganization in the other direction. This difference in three-dimensional space between the two charge reorganization procedures is, in turn, dictated by how the substrate and catalytic acid/base groups are organized in the active site of the enzyme.

Acknowledgment. We are grateful to funding from the North Carolina Biotechnology Center, the NIH program project on Computational Structural Biology at the University of North Carolina, and the National Science Foundation. Computer time from the North Carolina Super Computer Center has been used for the calculations.

JA9936619